ammonia on the corresponding monodentate α-keto carboxylate[3] or by elimination reactions on chelated *O*-acetylserinate or *S*-methylcysteinate to produce the chelated 2-iminopropanoate.[13] The chemistry described here provides an easy way of producing α-imino acidato complexes, provided side chain functionalities do not give undesired reactions with $SOCl_2$. Since the α-imino acidato chelate is a protected keto acid, this reaction could therefore constitute a relatively general synthesis of α-keto acids from their related α-amino acids (Scheme III). Should the free keto acid be required, then the complex could be decomposed by one of a variety of methods[24-26] and the keto acid isolated from the resulting mixture.

Analysis of the mechanism proposed here for the oxidation of non-glycine α-amino acidato complexes in the context of the reaction of $[Co(en)_2(Gly)]^{2+}$ (**2**) with $SOCl_2$ leads to the conclusion that these α-amino acidato complexes (**6a-j**) may not be good models for the $[Co(en)_2(Gly)]^{2+}$ complex (**2**) in this reaction. The structural difference, one α-proton instead of two in $[Co(en)_2(Gly)]^{2+}$, leads to other mechanistic possibilities, which are presently being explored.

Acknowledgment. Financial support for this work (to A.H.) from The Danish Natural Sciences Research Council is gratefully acknowledged. We are also grateful to the ANU Analytical Service for microanalyses.

Registry No. **6a**, 129448-02-8; **6b**, 129448-03-9; **6c**, 129448-04-0; **6d**, 129448-05-1; **6e**, 129448-06-2; **6f**, 129519-70-6; **6g**, 129466-73-5; **6h**, 129519-71-7; **6i**, 129466-74-6; **6j**, 129448-09-5; **7a**, 95098-08-1; **7b**, 129447-95-6; **7c**, 129447-97-8; **7d**, 129447-99-0; **7e**, 129448-00-6; **7f**, 129448-01-7; **7g**, 129448-08-4; **7h**, 129466-72-4; *S*-Ala, 17807-53-3; *S*-Tyr, 12557-24-3; *S*-Val, 17333-21-0; *S*-Glu, 138-18-1; *S*-Pro, 17781-82-7; Pip, 22560-49-2; *S*-Met, 44805-37-0; *S*-Lys, 17781-81-6.

(24) Clark, C. R.; Tasker, R. F.; Buckingham, D. A.; Knighton, D. R.; Harding, D. R. K.; Hancock, W. S. *J. Am. Chem. Soc.* **1981**, *103*, 7023.
(25) Knighton, D. R.; Harding, D. R. K.; Friar, M. J.; Hancock, W. S.; Reynolds, G. D.; Clark, C. R.; Tasker, R. F.; Buckingham, D. A. *J. Am. Chem. Soc.* **1981**, *103*, 7025.
(26) Keyes, W. E.; Legg, J. I. *J. Am. Chem. Soc.* **1976**, *98*, 4970.

Contribution from the Department of Chemistry, University of Calgary, Calgary, Alberta, Canada T2N 1N4

A Theoretical Study on the Insertion of Ethylene into the Cobalt-Hydrogen Bond

Louis Versluis, Tom Ziegler,* and Liangyou Fan

Received April 3, 1990

Two of the important elementary reaction steps in the hydroformylation process catalyzed by $HCo(CO)_3$ have been investigated by theoretical calculations based on the density functional theory. The first step involved the formation of the π complex $HCo(CO)_3(\eta^2\text{-}C_2H_4$ (I) from $HCo(CO)_3$ and C_2H_4. A total of three stable conformations of I were considered. All had a trigonal-bipyramidal structure. The most stable has C_2H_4 coordinated equatorially with the C=C olefin bond in the basal plane. The second (**1b**), which is 20 kJ/mol higher in energy, is also coordinated equatorially but has the C=C bond perpendicular to the basal plane. The third structure with C_2H_4 in the apical position (**2a**) is, on the other hand, 56 kJ/mol less stable than **1a**. The ethylene dissociation energy in **1a** was calculated to be 70 kJ/mol. The second step investigated involves the insertion of C_2H_4 into the Co-H bond of $HCo(CO)_3$, leading to the ethyl complex II. The most stable conformation of II, **4b**, has the ethyl group in the axial position and a β-hydrogen in the equatorial position interacting in an agostic manner with cobalt. Only 28 kJ/mol higher in energy is a second structure, **4a**, with the ethyl group in the equatorial position and a β-hydrogen in the axial position interacting in an agostic manner with cobalt. A third structure, **4c**, with the ethyl group in the axial position, but lacking an agostic interaction, was 39 kJ/mol higher in energy than **4b**. The energy profile for the insertion process was investigated by an approximate linear transit procedure, and it was found that the process (**1b** → **4a**) is exothermic (ΔE = -8 kJ/mol) with a modest activation barrier of not more than 6 kJ/mol.

Introduction

The oxo or hydroformylation reaction discovered in 1938 by Roelen is used on a large industrial scale[1] to convert olefins and synthesis gas into aldehydes. The process employs homogeneous catalysts based on cobalt[1] or rhodium.[2] The most commonly used (pre)catalyst is $HCo(CO)_4$, which is generated in situ from the hydrogenation of $Co_2(CO)_8$ by H_2.

A mechanism for the cobalt-based hydroformylation process was first proposed by Heck and Breslow[3] in 1961 (see Scheme I). The catalytic cycle in Scheme I consists of a number of elementary reaction steps (a-e), of which steps a and d have been investigated in a previous theoretical study.[4]

We shall here focus our interest on the coordination of olefin to the cobalt fragment, eq 1 (step b of Scheme I), as well as on the insertion process of C_2H_4 into the cobalt-hydrogen bond, eq 2 (step c of Scheme I).

$$HCo(CO)_3 + C_2H_4 \rightarrow HCo(CO)_3\text{-}C_2H_4 \quad (1)$$

$$HCo(CO)_3\text{-}C_2H_4 \rightarrow Co(CO)_3\text{-}C_2H_5 \quad (2)$$

Scheme I

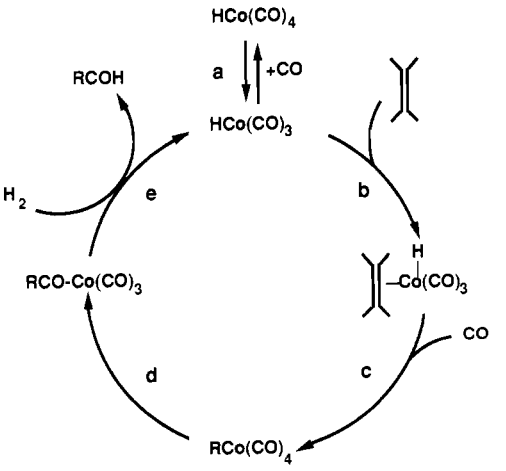

Not only is the study of these reactions important for the hydroformylation process as discussed here, but it is, on a more general basis, also relevant to the catalytic hydrogenation and isomerization of olefins, since the same elementary reaction steps have been proposed for these processes.[5] Experimental findings

(1) (a) Heck, R. F. *Adv. Organomet. Chem.* **1966**, *4*, 243. (b) Orchin, M.; Rupilius, W. *Catal. Rev.* **1972**, *6*, 85. (c) Orchin, M. *Acc. Chem. Res.* **1981**, *14*, 25.
(2) Pino, P.; Piacenti, F.; Bianchi, M. In *Organic Synthesis via Metal Carbonyls*; Wender, I., Pino, P., Eds.; Wiley: New York, 1977; Vol. II, pp 43-135.
(3) Heck, R. F.; Breslow, D. S. *J. Am. Chem. Soc.* **1961**, *83*, 4023.
(4) Versluis, L.; Ziegler, T.; Baerends, E. J.; Ravenek, W. *J. Am. Chem. Soc.* **1989**, *111*, 2018.
(5) Collman, J. P.; Hegedus, L. S. In *Principles and Applications of Organotransition Metal Chemistry*; Kelly, A., Ed.; University Science Books: Mill Valley, CA, 1980.

0020-1669/90/1329-4530$02.50/0

suggest that the migration of a hydride to a coordinated olefin group is very facile.[5] In fact, the hydride–olefin insertion reaction has, with a few exceptions,[6] rarely been directly observed. As a consequence, metal complexes containing both hydride and olefin are scarce. There have been a number of theoretical studies, at different levels of theory (EHT,[7] CNDO/2,[8] HF[9,10]), dealing with the electronic structures and geometries of π complexes of metal–hydrides with ethylene. Also, some results on the structures of coordinatively unsaturated metal complexes containing an ethyl ligand are available.[10,11] Two recent ab initio Hartree–Fock (HF) studies have been carried out on the hydride–ethylene insertion reactions of rhodium systems.[11] The only theoretical investigation on the cobalt species given in eqs 1 and 2, respectively, is a HF study by Antolovic and Davidson.[10]

We will here investigate steps b and c of Scheme I using the Hartree–Fock–Slater method.[12,13] The emphasis of the investigation lies on the identification of the equilibrium geometries and the relative energies of stable configurations of the π complex $HCo(CO)_3$–C_2H_4 and the coordinatively unsaturated intermediate $Co(CO)_3$–C_2H_5. The energy profile of the ethylene insertion into the Co–H bond will be modeled by an approximate linear transit procedure.

Computational Details

The calculations were all based on the Hartree–Fock–Slater (HFS) model as implemented by Baerends et al.,[12,13] where we have used the latest version of the fully vectorized HFS–LCAO–STO program due to Ravenek.[13b] The bonding energies were calculated by the generalized transition-state method[14] in conjunction with Becke's[15b] nonlocal exchange corrections as well as corrections to allow for correlations between electrons of different spins.[15a] The numerical integration scheme employed in this work was formulated by Becke.[16] The exchange factor[12] α_{ex} was taken as 0.7 in the pure HFS calculations[12] whereas a value of $^2/_3$ was adopted[15b] in calculations involving nonlocal exchange[15b] and local correlation corrections.[15a]

An uncontracted triple-ζ STO basis set[17] was used for the 3s, 3p, 3d, 4s, and 4p shells of cobalt. The 2s and 2p shells of C and O and the 1s shell of H were described by a double-ζ STO basis[17] set that was extended with one polarization function (2p on H and 3d on C and O). The electrons in the shells of lower energy on Co, C, and O were considered as core electrons and treated by the frozen-core approximation according to Baerends et al.[12,13a] All molecular structures were optimized within the C_s symmetry group. The geometry optimizations were carried out according to the algorithm developed by Versluis[18] and Ziegler. Calculations on metal carbonyls,[19] binuclear metal complexes,[20] and alkyl and hydride complexes,[21] as well as complexes containing M–L bonds for a number of different ligands,[22] have shown that the approximate density functional method employed here affords metal–ligand and metal–metal bond energies of nearly chemical accuracy (±5 kcal mol^{-1}). Approximate density functional methods have also been tested in connection with vibrational frequencies,[23] conformational energies,[4] and triplet–singlet separations.[24] More than 50 molecular structures optimized by the approximate density functional theory have been compared with experimental results.[18] The agreement between experimental and approximate density functional results is in most cases excellent.

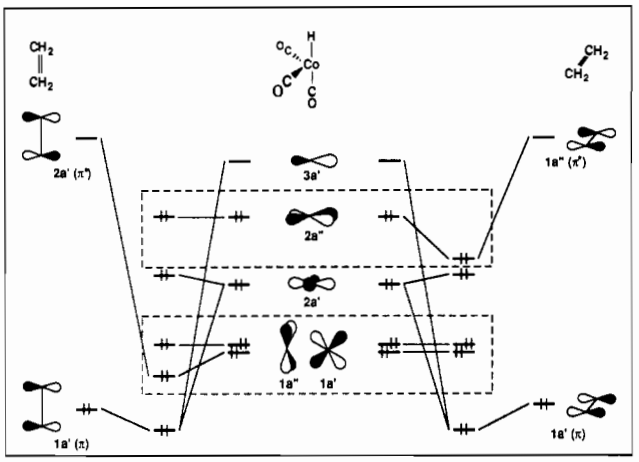

Figure 1. Diagram of the orbital interaction between the cobalt fragment and ethylene. The orbital notations are according to the C_s symmetry group. $HCo(CO)_3$ has a butterfly geometry with H along the apical axis. Ethylene is perpendicular to the basal plane at the left and coplanar at the right.

Molecular and Electronic Structure of $HCo(CO)_3(\eta^2\text{-}C_2H_4)$

The second step in the catalytic cycle of the oxo process (see step b of Scheme I) is the formation of a π complex between the unsaturated 16-electron cobalt intermediate $HCo(CO)_3$ and an ethylene molecule. We[4] have previously established that $HCo(CO)_3$ has three stable conformers, I–III, on the HFS energy surface with the relative order of stability, I (0) > II (38 kJ mol^{-1}) > III (69 kJ mol^{-1}).

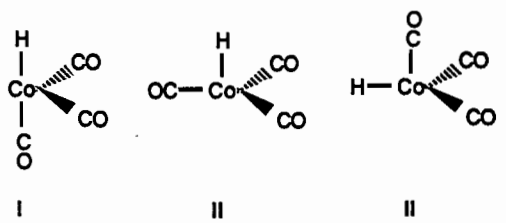

I II II

Of prime interest here will be the interaction of ethylene with the most stable conformer, I, since I can be expected to be predominantly present during the hydroformylation process. From I, two conceivable adducts can be constructed, one with the ethylene molecule coplanar to the basal plane, **1a**, and one with ethylene perpendicular to it, **1b**. The reaction of the trigonal-

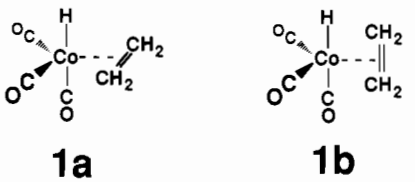

1a **1b**

shaped conformer, II, with C_2H_4 is not considered here, since the

(6) Werner, H.; Feser, R. *Angew. Chem., Int. Ed. Engl.* **1979**, *18*, 157.
(7) Thorn, D. L.; Hoffmann, R. *J. Am. Chem. Soc.* **1978**, *100*, 2079.
(8) Grima, J. Ph.; Choplin, F.; Kaufmann, G. *J. Organomet. Chem.* **1977**, *129*, 221.
(9) (a) Koga, N.; Jin, S. Q.; Morokuma, K. *J. Am. Chem. Soc.* **1988**, *110*, 3417. (b) Daniel, C.; Koga, N.; Han, J.; Fu, X. Y.; Morokuma, K. *J. Am. Chem. Soc.* **1988**, *110*, 3773.
(10) (a) Antolovic, A.; Davidson, E. R. *J. Am. Chem. Soc.* **1987**, *109*, 5828. (b) Antolovic, D.; Davidson, E. R. *J. Am. Chem. Soc.* **1987**, *109*, 977. (c) Antolovic, D.; Davidson, E. R. *J. Chem. Phys.* **1988**, *88*, 4967. (d) Veillard, A.; Strich, A. *J. Am. Chem. Soc.* **1988**, *110*, 3793.
(11) (a) Koga, N.; Obara, S.; Morokuma, K. *J. Am. Chem. Soc.* **1984**, *106*, 4625. (b) Koga, N.; Obara, S.; Kitawa, K.; Morokuma, K. *J. Am. Chem. Soc.* **1985**, *107*, 7109.
(12) Baerends, E. J.; Ellis, D. E.; Ros, P. *Chem. Phys.* **1973**, *2*, 41.
(13) (a) Baerends, E. J. Ph.D. Thesis, Vrije Universiteit, Amsterdam, 1975. (b) Ravenek, W. In *Algorithms and Applications on Vector and Parallel Computers*; Riele, H. J. J., Dekker, Th. J., van de Vorst, H. A., Eds.; Elsevier: Amsterdam, The Netherlands, 1987.
(14) (a) Ziegler, T.; Rauk, A. *Theor. Chim. Acta* **1977**, *46*, 1. (b) Ziegler, T. Ph.D. Thesis, University of Calgary, Calgary, Canada, 1978.
(15) (a) Stoll, H.; Golka, E.; Preuss, H. *Theor. Chim. Acta* **1980**, *55*, 29. (b) Becke, A. D. *J. Chem. Phys.* **1986**, *84*, 4524.
(16) Becke, A. D. *J. Chem. Phys.* **1988**, *88*, 2547.
(17) (a) Snijders, G. J.; Baerends, E. J.; Vernooijs, P. *At. Nucl. Data Tables* **1982**, *26*, 483. (b) Vernooijs, P.; Snijders, G. J.; Baerends, E. J. Slater Type Basis Functions for the whole Periodic System. Free University of Amsterdam: Amsterdam, The Netherlands, 1981 (internal report).
(18) Versluis, L.; Ziegler, T. *J. Chem. Phys.* **1988**, *88*, 322.
(19) Ziegler, T.; Tschinke, V.; Ursenbach, C. *J. Am. Chem. Soc.* **1987**, *109*, 4825.
(20) Ziegler, T.; Tschinke, V.; Becke, A. *Polyhedron* **1987**, *6*, 685.
(21) (a) Ziegler, T.; Tschinke, V.; Becke, A. *J. Am. Chem. Soc.* **1987**, *109*, 1351. (b) Ziegler, T.; Cheng, W.; Baerends, E. J.; Ravenek, W. *Inorg. Chem.* **1988**, *27*, 3458. (c) Ziegler, T.; Tschinke, V.; Baerends, E. J.; Snijdes, J. G.; Ravenek, W. *J. Phys. Chem.* **1989**, *93*, 3050.
(22) Ziegler, T.; Tschenke, V.; Versluis, L.; Baerends, E. J.; Ravenek, W. *Polyheron* **1988**, *7*, 1625.
(23) Fan, L.; Versluis, L.; Ziegler, T.; Baerends, E. J.; Ravenek, W. *Int. J. Quantum Chem.* **1988**, *S22*, 173.
(24) Ziegler, T.; Rauk, A.; Baerends, E. J. *Theor. Chim. Acta* **1977**, *43*, 261.

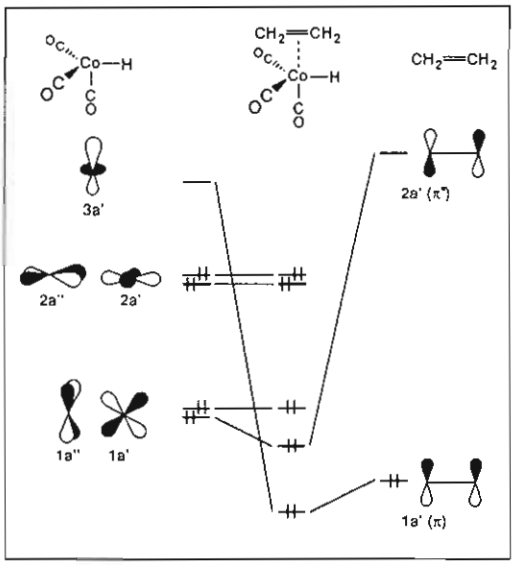

Figure 2. Diagram of the orbital interaction between the cobalt fragment and ethylene. The orbital notations are according to the C_s symmetry group. $HCo(CO)_3$ has a trigonal-pyramidal geometry where H is coordinated in the basal site. Ethylene is in the axial position and parallel to the Co–H bond.

resulting π complex has the hydride and the ethylene ligands trans to each other, which makes this species an unlikely candidate for the subsequent insertion reaction of C_2H_4 into the Co–H bond. The remainig stable configuration of $HCo(CO)_3$, III, can form the structures **2a** and **2b** with ethylene. We will only include

2a **2b**

structure **2a** in our calculations, since **2b** would have to rearrange to **2a** in order to have the ethylene molecule ideally positioned for the hydride migration.

Let us first discuss structures **1a**, **1b**, and **2a**, respectively, on a qualitative basis. The interaction of an unsaturated alkene molecule with a transition-metal fragment is commonly described by using the Dewar–Chatt–Duncanson model.[25] The bonding is mainly attributed to the interaction of the occupied π orbital and the vacant antibonding π^* orbital on ethylene with the metal fragment. Figure 1 shows the interaction diagram between the orbitals of $HCo(CO)_3$ in its most stable butterfly-shaped configuration, I, and the frontier orbitals of ethylene for both orientations according to structures **1a** and **1b**, respectively. The related interaction diagram for structure **2a** is given in Figure 2. Ethylene is bonded to the cobalt fragment through an interaction of the occupied 1a'(π) orbital on C_2H_4 with the LUMO 3a' on Co and a back-bonding interaction between an occupied metal orbital and the antibonding π^* orbital on ethylene (see Figures 1 and 2).

The former interaction is for all three structures (**1a**, **1b**, and **2a**) approximately equivalent and is expected, according to simple perturbation theory, to be weak, since there is a large energy gap between the orbitals. The relative strengths of the Co–C_2H_4 bonds for the three structures is, therefore, determined by the degree of back-bonding. We get then the well-known result[26] that structure **1a** with ethylene coplanar to the equatorial plane is lower in energy than **1b**, since the energy gap between 1a''(π^*) and the high-lying σ antibonding metal orbital 2a'' of structure **1a** is smaller than the corresponding gap between 2a'(π^*) and 1a' for

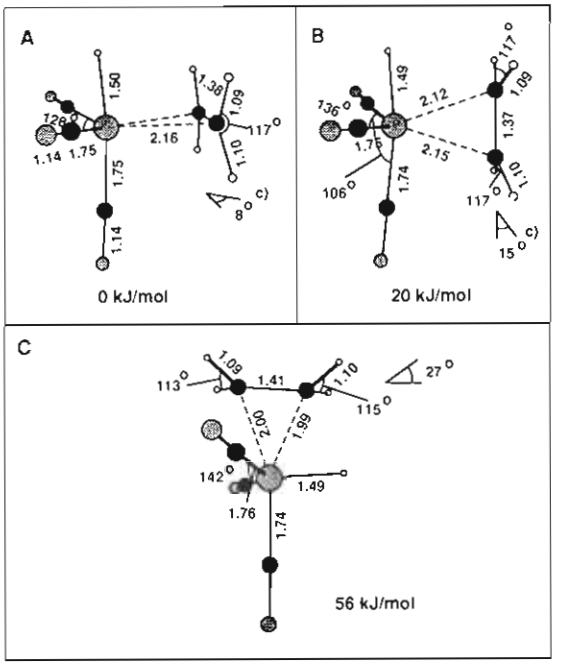

Figure 3. Optimized structures and relative energies of η^2-$HCo(CO)_3$–C_2H_4. Bond distances are in angstroms. The energies are relative to structure A, which was set arbitrarily to zero. The 27° angle given in part C is the deviation of the ethylene molecule from planarity.

structure **1b** (see Figure 1). The ethylene–cobalt bond strength of $HCo(CO)_3$–C_2H_4 with ethylene along the axial axis, **2a**, should be similar to the corresponding value for structure **1b**, since the orbital interactions are more or less identical. However, the overall stability favors structure **1b**, because the coordinatively unsaturated metal fragment, I, in **1b** is lower in energy than the related fragment, III, in **2a**. Thus, we expect the stabilities of the structures of **1a**, **1b**, and **2a**, respectively, to follow the order **1a** > **1b** > **2a**.

The optimization of the structures in question revealed that all three of them represent local minima on the HFS energy surface with a positive Hessian optimization matrix. The optimized geometries are given in Figure 3. As antipicated, the π complex with ethylene lying in the equatorial plane, Figure 3A, is lowest in energy, while complexes **1b** (Figure 3B) and **2a** (Figure 3C) are less stable by 20 and 56 kJ/mol, respectively. Our results are contrasted by a recent HF study[10b] on the same cobalt complexes, where configuration **1b** was found to be 45 kJ/mol higher in energy than structure **1a** and complex **2a** was predicted to be the most stable species with an energy 5 kJ/mol below that of **1a**. The prediction that the complex with the hydride ligand in the equatorial position is lowest in energy follows closely the results of the same authors[10b] on the related tetracarbonyl complex, $HCo(CO)_4$, where they find $HCo(CO)_4$ of C_{2v} symmetry to be favored over the C_{3v} configuration, which contrasts experimental observations. Antolovic[10c] and Davidson have recently analyzed the importance of electron correlation for a description of the electronic structure in $HCo(CO)_4$ and $HCo(CO)_3$. Veillard[10d] and Strich have studied the photochemistry of $HCo(CO)_4$ based on high-level CI calculations.

Antolovic and Davidson[10b] offer also some CI results on the ethylene π-complexes. They find now **1b** to be 95 kJ/mol higher in energy than **1a**, and **2a** to be 42 kJ/mol above **1a**. However, these results are difficult to interpret since they were obtained for the HF geometries, which typically are unreliable for transition-metal complexes.[27]

Our calculated values seem to comply with the experimental observation that olefins insert readily into the metal–hydrogen bond. That is, the π complexes of structures **1b** and **2a** must have

(25) (a) Dewar, M. J. S. *Bull. Soc. Chim. Fr.* **1951**, *18*, C71. (b) Chatt, J.; Duncanson, L. A. *J. Chem. Soc.* **1953**, 2939.
(26) Rossi, A. R.; Hoffmann, R. *Inorg. Chem.* **1975**, *14*, 365.
(27) (a) Luthi, H. P.; Siegbahn, P. E. M.; Almlof, J. *J. Phys. Chem.* **1985**, *89*, 2156. (b) Luthi, H. P.; Ammeter, J. A.; Almlof, J.; Faegri, K. *J. Chem. Phys.* **1982**, *77*, 2002.

energies comparable to those of the most stable species, **1a**, since the latter has to rearrange to either one of them in order to bring the ethylene molecule into a position close to the hydride prior to the insertion process. The present method calculates the energy difference between **1a** and **1b** to be 20 kJ mol^{-1}. This value is small compared to observed olefin rotation barriers in d^8 ML$_n$(olefin) complexes, which typically are in the range 40–60 kJ mol^{-1}. However, even a somewhat higher value of 40 kJ mol^{-1} would still make the rearrangement **1a** → **1b** a viable step in the insertion process.

The optimized structures in Figure 3 have also some interesting geometrical features. Most notable is the bending-back of the hydrogen atoms on C_2H_4 as well as the elongation of the ethylene double bond with respect to a bond length of 1.33 Å for the free molecule. The increase of the bond length can, as in the carbonyl case, be attributed to the population of the antibonding π^* orbital on C_2H_4 through the back-bonding mechanism, as illustrated in Figures 1 and 2. The bond length is, however, also affected by the degree of distortion of the ethylene molecule from planarity (vide infra).

The bending-back of the alkene substituents upon formation of a metal π comlex is a well-documented effect.[28] The distortion will raise the energy level of the ethylene π orbital and lower the corresponding π^* orbital, as is illustrated by **3**. This is very

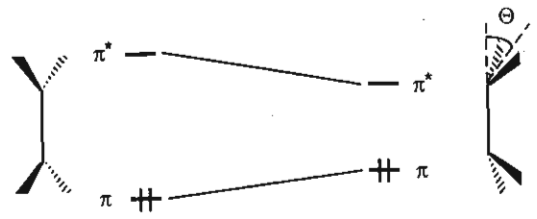

3

desirable, since it will strengthen the bonding between the metal fragment and ethylene by decreasing the energy gaps of the respective interacting orbitals (see Figures 1 and 2). The degree by which the hydrogen atoms of C_2H_4 bend away from the metal fragment depends on the energy gap between the interacting orbitals.

From our simple orbital temperature diagrams (Figure 1 and 2) we would then conclude that the π complex of configuration **1a** will experience the smallest distortion, since the energy gap between orbital 1a″(π^*) and 2a″ is in comparison not as large as for the other orbital interactions. We find from our calculations the following values for the distortion angle Θ of **3**: Θ = 8° for complex **1a**, Θ = 15° for **1b**, and Θ = 27° for **2a**. Structure **2a**, which features the largest distortion angle, also possesses the longest ethylene C–C bond. This is in accordance with the prediction that bending the substituents will elongate the bond length. On the other hand, the order of the C–C bond lengths seems to be inverted for structures **1a** and **1b**, where **1a** has a longer bond than **1b** but a smaller distortion angle. This is due to the fact that the π complex of configuration **1a** has a stronger back-bonding component than structure **1b**; hence, the bond elongation resulting from the population of the antibonding π^* orbital on ethylene outweighs the corresponding effect due to the bending of the hydrogen atoms.

We have also carried out some calculations on the strength of the cobalt–ethylene bond. Thus the cobalt–ethylene bond strength $\bar{D}$(Co–C_2H_4) for the complex of structure **1a** was found to be 92 kJ/mol. This value, however, corresponds to a dissociation process in which the separating fragments have not been allowed to relax. Including the relaxation energy, which we estimate to be 20 kJ/mol, affords a bond energy of 70 kJ/mol for **1a**. Experimental values range from 149 kJ/mol for η^2-Fe(CO)$_4$–C_2H_4–C_2H_4[29] to 49 kJ/mol for the bonding of ethylene with Ir(PPh$_3$)$_2$COCl.[30]

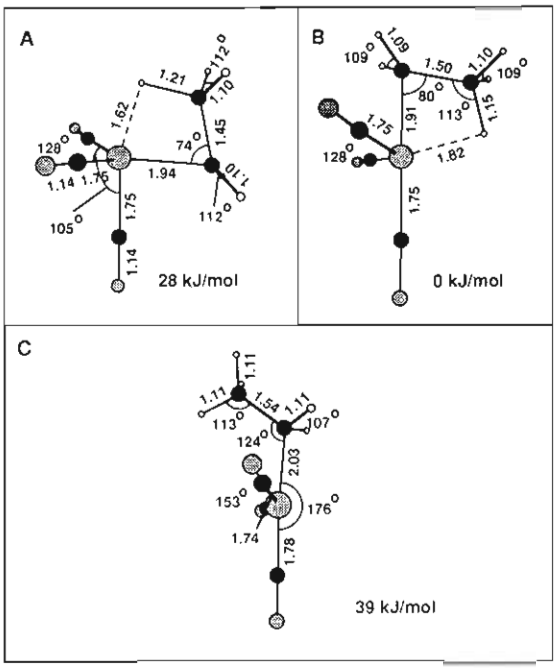

Figure 4. Optimized structures and relative energies of C_2H_5–Co(CO)$_3$. Bond distances are in angstroms, and angles, in degrees. The energies are relative to the most stable structure B, which was set arbitrarily to zero.

There are, to our knowledge, no data available that are relevant to the molecular systems studied here.

Molecular and Electronic Structure of (CO)$_3$Co–C_2H_5

The next step of the catalytic cycle is the intramolecular migratory insertion of ethylene into the metal–hydride bond, step c of Scheme I.

$$(CO)_3HCo–C_2H_4 \rightarrow (CO)_3Co–C_2H_5 \qquad (3)$$

As mentioned in the Introduction, this type of reaction has been proposed for numerous catalytic processes, but it has only in a few isolated cases been possible to study the hydride–olefin insertion directly by experimental technqiues.[31]

We have carried out calculations on some of the structures that are expected to be formed during the insertion process. Our attention will be focused on the coordinatively unsaturated intermediates that arise from the migration of the hydride ligand to the ethylene group in complex **1b**, **1b** → **4a**, and from complex

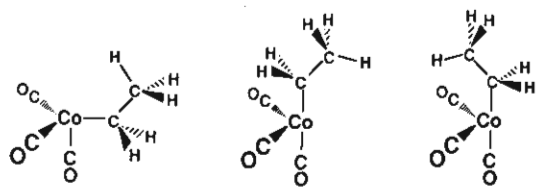

4a **4b** **4c**

2a, **2a** → **4b**. For the more stable π complex, **1b**, we will also consider the intermediate that can result from a direct insertion of the ethylene ligand into the Co–H bond, **1b** → **4c**. We note that the intermediate **4c** can also be reached by a simple rotation of the ethyl group in structure **4a** or **4b**, respectively.

The optimized geometries are given in Figure 4. Similar to the case of the π complexes in the preceding section, we find the relative energies to be close, with complex **4b** lowest in energy and structures **4a** and **4c** less stable by 28 and 39 kJ/mol, respectively. An interesting observation is the formation of an agostic interaction between an ethyl hydrogen atom and the metal center

(28) Ittel, S. D.; Ibers, J. A. *Adv. Organomet. Chem.* **1976**, *14*, 33.
(29) Skinner, H. A.; Connor, J. A. *Pure Appl. Chem.* **1985**, *57*, 79.
(30) Mondal, J. U.; Blake, D. M. *Coord. Chem. Rev.* **1982**, *47*, 205.
(31) Werner, H.; Feser, R. *Angew. Chem., Int. Ed. Engl.* **1979**, *18*, 157.

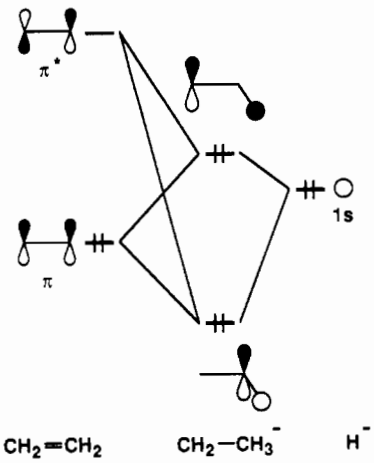

Figure 5. Schematic diagram of the interaction between ethylene and H.

for the intermediates of configurations **4a** and **4b** (Figure 4A,B). The shortest metal–hydrogen distance (1.62 Å) is found in structure **4a**. This distance is only 0.12 Å longer than the Co–H bond distance in the parent complex **1b**. The bond length of the agostic hydrogen with the corresponding carbon atom of the ethyl ligand is, on the other hand, substantially elongated with R(H–C) = 1.21 Å in comparison to a normal ethyl C–H bond length of 1.11 Å.[32] The C–C bond distance in the ethyl group is 1.45 Å, which is somewhat longer than the corresponding value in the parent structure **1b** (1.37 Å), but it is still substantially shorter than the C–C bond length of an undistorted ethyl group (1.53 Å[32]).

Also, the bond angle Co–C_{et}–C_{et} is 74°, considerably smaller than the expected value of about 109° for a normal ethyl ligand. The optimized molecular parameters of structure **4a** (Figure 4A) clearly indicate that the π–bond character of the initial ethylene ligand has been retained to a large extent. This is also underlined by the small calculated energy difference of 8 kJ/mol between the parent structure **1b** and complex **4a**.

As mentioned above, also the ethyl intermediate of configuration **4b** forms an agostic interaction. As in the case of **4a**, the molecular parameters of **4b** lie between the values of the pure π complex (**2a**) and the expected values of a standard ethyl ligand. However, the structural parameters in **4b** are now closer to the values of a normal ethyl ligand. For example, the bond distance of the hydrogen atom that forms the agostic interaction with the ethyl carbon atom is 1.15 Å, only 0.04 Å longer than the expected value. As a consequence, the agostic interaction is less pronounced, which manifests itself in a by 0.20 Å larger distance between the agostic hydrogen and the cobalt nucleus. In addition, the ethyl intermediate (**4b**) is now 62 kJ/mol lower in energy than the parent structure (**2a**); thus the energy difference is much larger than before. An explanation for this can be found from the fact that the initial π complex of configuration **2a** is, in comparison to the conformers **1a** and **1b**, high in energy, as discussed in the previous section, while the intermediate **4b** adopts a butterfly structure, which is predicted[33] to be the most stable configuration for a d^8 complex.

The interaction of an alkyl CH bond with the metal center of a transition-metal complex has been observed experimentally in several instances and is proposed to play an important role in CH activation.[34] Koga et al.[35] have, at the HF level of approximation, given a theoretical account on the CH···M interaction of transition-metal complexes (M = Ti, Ni, Pd) containing an ethyl

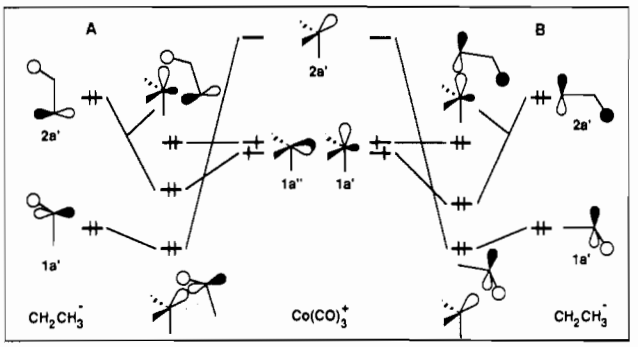

Figure 6. Diagram of the orbital interaction between the cobalt fragment of $Co(CO)_3^+$ and the distorted ethyl group $CH_3CH_2^-$. The orbital notations are according to the C_s symmetry group. The geometry of the ethyl group in C_2H_5–$Co(CO)_3$ is optimized. Ethyl is coordinated in the basal site (A) and in the axial site (B).

ligand. They conclude from their work that the driving force of the formation of an agostic interaction results from an electron donation of the C–H σ-bond to an empty vacant orbital on the metal center.

We can gain a qualitative understanding of the bonding by investigating the orbital interactions between the metal fragment $Co(CO)_3^+$ and the ethyl fragment $CH_3CH_2^-$. The frontier orbitals of a d^8 $M(CO)_3$ species are well documented in the literature[36] and are given here in Figure 6. The dominant orbitals of the distorted ethyl group can be constructed from an interaction of ethylene with hydrogen, which is illustrated in Figure 5. The hydride s orbital interacts with the occupied π orbital on C_2H_4, causing a four-electron destabilization. Both resulting orbitals can be stabilized by mixing in the π^* orbital, which in particular relieves the antibonding combination of the s and the π orbital (**5**).

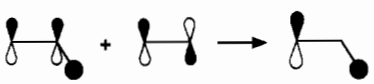

5

We can now analyze how the distorted ethyl group is stabilized by the cobalt fragment. Figure 6 shows the interaction of the $Co(CO)_3^+$ fragment with $CH_3CH_2^-$ in the equatorial position (Figure 6A) and in the axial position (Figure 6B). In both orientations the orbitals of $CH_3CH_2^-$ can interact very well with the metal fragment. Orbital $1a'_{CH_3CH_2}$, which represents the C–H σ-bond, overlaps with $2a'_{Co(CO)_3}$, which is primarily 4p in character. The second ethyl orbital, $2a'_{CH_3CH_2}$, has the right symmetry to form a stabilizing interaction with the metal orbital $1a'_{Co(CO)_3}$. We note here in particular that $2a'_{CH_3CH_2}$ can interact with both lobes on $1a'_{Co(CO)_3}$. Some of the structural differences between the ethyl group in complex **4a** and in **4b** can also be understood from the orbital interaction diagram in Figure 6. Most notable is the difference of the distance between the agostic hydrogen atom and the cobalt nucleus (0.02 Å). While both complexes have basically identical orbital interactions between $1a'_{CH_3CH_2}$ and $2a'_{Co(CO)_3}$ (see Figure 6A,B), they feature markedly different interactions between the orbitals $2a'_{CH_3CH_2}$ and $1a'_{Co(CO)_3}$. In structure **4a** the localized hydrogen 1s function in orbital $2a'_{CH_3CH_2}$ points toward the apical position and overlaps, therefore, with the larger lobe of $1a'_{Co(CO)_3}$ (Figure 6A), while in **4b** the corresponding interaction involves the smaller lobe of $1a'_{Co(CO)_3}$ (Figure 6B). Thus, the H–Co interaction in **4a** is expected to be stronger, which is expressed by a smaller H–Co internuclear distance.

The formation of an agostic interaction is not observed for the ethyl intermediate of configuration **4c**, where the ethyl ligand is, in comparison to structure **4b**, rotated by 180°. The methyl group in the ethyl ligand is now pointing away from the vacant site of the coordinatively unsaturated intermediate. As a consequence,

(32) Callomon, J. H.; Hirota, E.; Kuchitsu, K.; Lafferty, W. J.; Maki, A. G.; Porte, C. S. In *Landolt-Bornstein*; Hellwege, K. H.; Hellwege, A. M., Eds.; Springer: Berlin, 1976; Vol. 7.
(33) Elian, M.; Hoffmann, R. *Inorg. Chem.* **1975**, *14*, 1058.
(34) Brookhart, M.; Green, M. L. H. *J. Organomet. Chem.* **1983**, *250*, 395.
(35) (a) Koga, N.; Obara, S.; Morokuma, K. *J. Am. Chem. Soc.* **1984**, *106*, 4625. (b) Koga, N.; Obara, S.; Kitaura, K.; Morokuma, K. *J. Am. Chem. Soc.* **1985**, *107*, 7109.
(36) Berke, H.; Hoffmann, R. *J. Am. Chem. Soc.* **1978**, *100*, 7224.

Table I. Calculated Reaction Energies for the Migratory Insertion Process

R ➡ P		ΔE (kJ/mol)
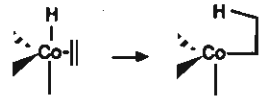	**1b → 4a**	**-8**
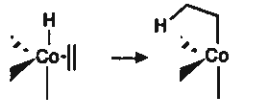	**1b → 4c**	**3**
	**2a → 4b**	**-62**

the orbital that represents the C–H σ-bond, $1a'_{CH_3CH_2}$ of Figure 6, is now unable to interact with the metal orbitals. Furthermore, only the localized p function of the second ligand orbital, $2a'_{CH_3CH_2}$, can overlap with the metal orbital $1a'_{Co(CO)_3}$, while the s-type function on $2a'_{CH_3CH_2}$ fails to find an orbital partner on the metal center. Therefore, the ethyl ligand cannot form an agostic interaction but adopts a standard configuration with sp^3-hybridized carbon atoms. However, structure **4c** is able to stabilize itself somewhat by opening the bond angle between the equatorial carbonyl ligands (128° in **4b** → 153° in **4c**). This effect was also observed in our previous investigation[4] of the formyl intermediates, $HC(O)Co(CO)_3$.

The Migratory Insertion Step

Finally, we shall discuss here the energetics as well as the energy profile of the intramolecular olefin insertion process. The energy profile will be approximated by a linear transit. The principle behind the linear transit is simple and can be illustrated by considering the process **1b** → **4a**. The two structures **1b** and **4a** can be characterized by a common set of internal coordinates $\{\alpha_i, i = 1, n\}$, and **1b** is transformed into **4a** by changing the internal coordinates from the values $\{\alpha_i^r, i = 1, n\}$ they had in **1b** to the values $\{\alpha_i^p, i = 1, n\}$ they have in **4a** by $\{\Delta\alpha_i, i = 1, n\}$. The transformation from **1b** to **4a** is accomplished in a linear transit by changing the internal coordinates by increments of $\{\Delta\alpha_i/m, i = 1, n\}$ a total of m times.

First, let us look at the relative energies between the reactants and products. Table I reveals, as noted in the previous section, that the hydride migration in the ethylene π complex of configuration **1b** (**1b** → **4a**) is slightly exothermic with $\Delta E = -8$ kJ/mol. The alternative reaction where the ethylene group inserts directly into the Co–H bond (**1b** → **4c**) exhibits also a small energy difference between reactant and product with $\Delta E = 3$ kJ/mol. At first sight, this seems to be somewhat surprising, since the ethyl intermediate (**4c**) in the latter reaction does not form a stabilizing agostic interaction. However, complex **4c** has the ethyl ligand in the apical position, forming therefore a butterfly-shaped structure, which is, as mentioned earlier, the most stable configuration for a d^8 complex. On the other hand, structure **4a** has the ethyl ligand attached in the less favorable equatorial position. It makes up for the higher energy by stabilizing itself through the agostic interaction; as a result, the enthalpies of the two reaction modes are similar. The hydride migration in the π complex with ethylene in the axial position (**2a** → **4b**) is, in contrast to the former reactions, strongly exothermic with $\Delta E = -62$ kJ/mol. The large exothermicity stems from the fact that the π complex **2a** is higher in energy than **1b** while structure **4b** forms the most stable ethyl intermediate (see Figure 9). Consequently, the energy difference for the reaction **2a** → **4b** is larger than that for the corresponding process **1b** → **4a**. Antolovic and Davidson[10a] found, at the HF level, for the first reaction, **1b** → **4a**, $\Delta E = -107$ kJ/mol and, for the second reaction **2a** → **4b**, $\Delta E = -46$ kJ/mol. They also provided some CI energies ($\Delta E = -79$ kJ/mol for **1b** → **4a** and $\Delta E = -4$ kJ/mol for **2a** → **4b**), which were however

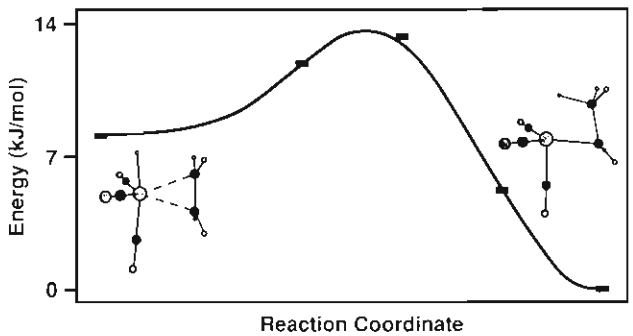

Figure 7. Energy profile of the hydride migration to the ethylene group in η^2-$HCo(CO)_3$-C_2H_4 (reaction **1a** → **4a**). The energy zero point refers to structure **4a**.

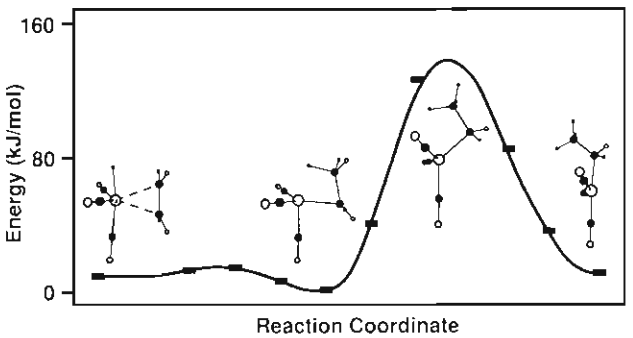

Figure 8. Energy profile of the hydride migration and the subsequent ethyl rearrangement for η^2-$HCo(CO)_3$-C_2H_4 (reaction **1a** → **4a** → **4c**). The energy zero point refers to structure **4a**.

calculated for the HF geometries. The fact that the ab initio calculations predicted reaction **1b** → **4a** to be more exothermic can be traced to the fact that they found, in contrast to our results, the π complex of configuration **2a** to be considerably lower in energy than **1b**. Koga et al.[9a] found in a HF study on the migratory olefin insertion in $Rh(H)(C_2H_4)(CO)_2(PH_3)$ exothermicities ranging from −57 to −142 kJ/mol, while Daniel et al.[9b] found the corresponding reaction in $Rh(H)(Cl)(PH_3)_2(C_2H_4)$ to be endothermic with $\Delta E \approx 80$ kJ/mol.

In the following, we shall investigate the energy profile of the intramolecular migratory insertion process by tracing the HFS energy surface by a linear transit procedure. As mentioned earlier, this method will only approximate the reaction path and yields an upper bound to the activation energy. We will restrict our considerations to the migratory process involving the π complex of configuration **1b**. Figure 7 shows the energy profile of the hydride migration **1b** → **4a**. We find the reaction to have a very small activation barrier, $\Delta E^{\ddagger}$, of only 6 kJ/mol. This is in sharp contrast to the results of Antolovic and Davidson,[10a] who found 61 kJ/mol at the HF level and 73 kJ/mol at the CI level of theory. The large discrepancy between the HFS and the ab initio results can be attributed to the fact that the latter methods seem not to predict an agostic interaction between the shifted hydride ligand and the metal center in the final structure. As a consequence, the linear transit procedure in the ab initio study yields a transition state that has a large H–Co distance as well as a large $H–C_{Et}$ distance. In other words, the H–Co bond has to be stretched considerably before the molecular system can be stabilized through the formation of a C–H bond. On the other hand, the Co–H bond of the reaction modeled in Figure 7 is not broken during the migration process, which results in a low activation energy.

We will consider next the ethyl conversion, in which the ethyl ligand moves from the equatorial position to the axial site, **4a** → **4c**. The interest in this rearrangement stems from the observation that the subsequent reaction of **4c** with an incoming CO molecule (see step c of Scheme I) will yield a coordinatively saturated species with the alkyl group in the axial position while the corresponding reaction of structure **4a** with CO results in the less stable complex with C_2H_5 in the basal plane. The energy profile for the ethyl

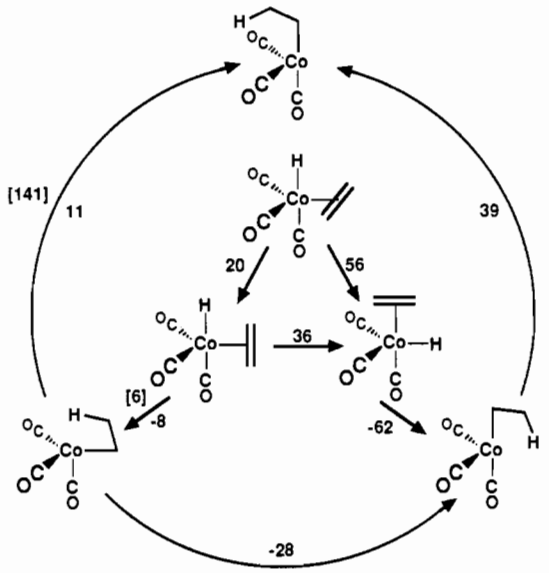

Figure 9. Energy requirements for the insertion of ethylene into the Co–H bond of η^2-$HCo(CO)_3$–C_2H_4. All energies are in kJ/mol. The numbers of brackets represent the activation energies for the reaction in the direction of the arrows. The numbers without brackets stand for the energy difference between two isomers, where a positive value indicates that the resulting complex is higher in energy.

rearrangement, obtained by the approximate linear transit procedure, is given in Figure 8. We find for **4a** → **4c** a considerable activation barrier ΔE^* of 130 kJ/mol. This value is comparable to the activation barrier (97 kJ/mol) that was found in our previous study[4] for the related process where, instead of an ethyl group, an acyl ligand is rotated from the equatorial to the axial orientation. The high energy barriers arise mainly from a destabilizing four-electron interaction between an occupied d-type orbital on the metal center and an occupied σ orbital on the ligand. The activation barrier of the ethyl conversion is further enhanced by the cleavage of the stable agostic interaction in complex **4a**. The high activation barrier indicates that under catlaytic conditions the ethyl conversion is probably superseded by the coordination of a CO molecule in the axial site. The coordinatively saturated alkyl intermediates can then rearrange to the most stable TBP configuration with the alkyl group in the apical position by a Berry pseudorotation for which the activation energy is predicted[9a] to be low.

Summary and Conclusions

We have investigated here the geometries of the π complexes that result from an interaction between ethylene and the coordinatively unsaturated cobalt complex $HCo(CO)_3$. Furthermore, the insertion of the coordinated ethylene group into the Co–H bond was also studied by determining the geometries of some of the insertion products as well as by evaluating the energy profile of the insertion mechanism by a linear transit procedure. The processes under investigation constitute the second and third reaction steps of the catalytic hydroformylation cycle shown in Scheme I.

Three π structures were considered. The one resulting from an interaction of C_2H_4 with the most stable configuration of $HCo(CO)_3$ (see Figure 3A), in which the C=C ethylene bond is in the basal plane (**1a**), was lowest in energy. The corresponding configuration with ethylene parallel to the axial axis (**1b**) was also found to be stable and only 20 kJ/mol higher in energy than **1a**. The third structure, with C_2H_4 in the apical position (**2a**), is, on the other hand, 56 kJ/mol less stable than the π complex of geometry **1a**. Calculations on the Co–C_2H_4 bond energy in structure **1a** yielded a value of 70 kJ/mol.

The migratory insertion process was studied for the π complexes of configurations **1b** and **2a**, which both have the ethylene group lined up with the Co–H bond. The ethyl intermediates, which have the shifted hydrogen atom pointing toward the vacated site, formed strong agostic interactions with the H atom bonded to both a carbon atom of the C_2H_4 ligand and the cobalt nucleus. The corresponding structural parameters of the ethyl ligand lie between the values of the π complex and the expected values of a standard ethyl group. We have modeled the energy profile of the hydride migration with the more stable ethylene π complex **1b** and found a small reaction energy ΔE of −8 kJ/mol associated with a very low activation barrier ΔE^* of only 6 kJ/mol. Thus, the molecule is very flexible and can shift easily between the π complex and the agostic ethyl intermediate. The low activation barrier can be attributed to the fact that, due to the formation of an agostic interaction, the cobalt–hydride bond is not broken during the migratory motion. The facility of the hydride migration to the ethylene ligand is in sharp contrast to the poor migratory ability of hydride toward a CO group.[4] We have in the present investigation only considered insertion of olefin to the Co–H bond from trigonal-bipyramidal structures. Thorn[7] and Hoffmann have previously shown, from calculations on the d^8 $PtHCl(PH_3)_2$ model systems, that square-pyramidal intermediates with the proper orientation ethylene and the hydride for facile insertion are too high in energy, in keeping with the fact that d^8 ML_4(olefin) complexes invariably adopt a TBP structure.

Acknowledgment. This investigation was supported by Natural Sciences and Engineering Research Council of Canada (NSERC). We also acknowledge access to the Cyber-205 installations at the University of Calgary.

Supplementary Material Available: Cartesian coordinates for the optimized structures in Figures 3 and 4 (4 pages). Ordering information is given on any current masthead page.